Epidermal SIRT1 and BDNF modulate mechanical allodynia in mouse models of diabetic neuropathy

Jennifer O'Brien*[2], Peter Niehaus*[1, 2], Juliana Remark[5], Mohammad Salimian[3,6], Yanni Kevas[3], Samuel Rubin[1,7], Tibor Kristian[4, 8], Krish Chandrasekaran[3, 8], Catherine Pei-Ju Lu[5], James W. Russell[3, 8], Cheng-Ying Ho[1, 2]

Department of Pathology, Johns Hopkins University School of Medicine, Baltimore, MD[1]; Department of Pathology[2], Neurology[3] and Anesthesiology[4], University of Maryland School of Medicine, Baltimore, MD; Hansj□rg Wyss Department of Plastic Surgery, Department of Cell Biology, New York University School of Medicine, New York, NY[5]; Department of Pathology, Orlando Health, Orlando, FL[6]; Department of Chemistry, College of William and Mary, Williamsburg, VA[7];

Baltimore Veterans Affairs Medical Center, Baltimore, MD[8]

*Equal contribution

Address correspondence to: Cheng-Ying Ho, Department of Pathology, Johns Hopkins University School of Medicine, 1800 Orleans St, M2101, Baltimore, MD 21287. Phone: 1-410-955-8378. Email: cho9@jh.edu

Abstract

Diabetic neuropathy (DN) is a debilitating disorder characterized by mechanical allodynia and sensory loss. It has traditionally been considered a small-fiber neuropathy, defined by the loss of free nerve endings in the epidermis. Free nerve endings, however, are nociceptors which may not be the only sensor for mechanical pain. To investigate the role of mechanoreceptors, specifically Meissner corpuscles, in the development of diabetic mechanical allodynia, our study focused on the keratinocyte-secreted brain-derived neurotrophic factor (BDNF) and its transcriptional regulator sirtuin 1 (SIRT1). Wild-type DN mice demonstrated decreased SIRT1 deacetylase activity, leading to a decrease in BDNF expression and Meissner corpuscle densities in foot skin. Epidermal *SIRT1* knockout (KO) mice developed exacerbated DN phenotypes including severe mechanical allodynia, markedly reduced Meissner corpuscles, and subcutaneous Aß axon degeneration. Among the major skin-derived neurotrophic factors, only BDNF was down-regulated in epidermal *SIRT1* KO mice. With similar KO phenotypes, epidermal BDNF appeared to belong to the same pathway as SIRT1 in modulating diabetic mechanical allodynia. Furthermore, mice overexpressing epidermal SIRT1 showed BDNF up-regulation and improved DN phenotypes, supporting an important role of epidermal SIRT1 and BDNF in skin sensory apparatus regeneration and functional recovery in the setting of diabetes.

Introduction

Diabetic neuropathy (DN) is a common complication of diabetes and prediabetes, affecting up to 50% of the adult patients (1). Patients develop symptoms such as mechanical allodynia, spontaneous pain, numbness, paresthesia, and dysautonomia, with mechanical allodynia (neuropathic pain) being one of the most common complaints (2). DN, particularly the distal symmetric polyneuropathy subtype, is classified as a small fiber neuropathy based on the clinical presentations and progressive loss of small nerve fibers seen on skin biopsies. Small fibers comprise of unmyelinated C fibers and small myelinated Aδ fibers (3) and are responsible for sensory perceptions such as temperature and nociceptive pain (4). Large myelinated sensory fiber alterations have also been reported in early DN (5–7), but are not well investigated. Among the sensory abnormalities experienced by DN patients, burning and blunt pressure pain has been attributed to sensitization of C fibers, whereas pricking sensation is linked to Aδ fiber injuries (8,9). Mechanical allodynia, in comparison, is thought to be triggered by activation of Aß fibers (10–12). In the inflammatory pain mouse model, Aβ fibers appear to cause mechanical allodynia by switching their phenotype to one resembling nociceptive C fibers, thereby enhancing central sensitization to innocuous stimuli (13). A study by Xu et al. showed that blockade of Aß and not C fibers successfully inhibited mechanical allodynia, highlighting the potential of targeting Aß fibers as a novel therapeutic strategy for neuropathic pain (11).

Aß mechanosensory neurons consist of slowly adapting (SA) and rapidly adapting (RA) low-threshold mechanoreceptors (LTMRs), which form sensory apparatus such as Merkel cell complexes, Ruffini endings, Meissner corpuscles and Pacinian corpuscles in glabrous (hairless) skin and longitudinal lanceolate endings in hairy skin (14). Among these Aß mechanosensory receptor end organs, Meissner corpuscles are the only one that possesses immunochemical

properties similar to nociceptors (15) in addition to their normal function of detecting gentle touch perception (16). Reduced densities of Meissner corpuscles have been observed in human patients of chemotherapy-induced peripheral neuropathy (17) and DN (18,19). Creigh et al. used in-vivo reflectance confocal microscopy to visualize Meissner corpuscles in DN patients, and detected decreased Meissner corpuscle densities early in the disease process (19). The finding suggests that Meissner corpuscle alterations may be used as a marker to monitor disease progression or treatment response in DN.

Meissner corpuscles are dually innervated by $TrkB^+$ and Ret^+ Aß mechanosensory afferents. A study by Neubarth et al. revealed loss of Meissner corpuscles and light touch perception in mice lacking TrkB in primary sensory neurons (16). Dhandapani et al. showed that photo-ablation of $TrkB^+$ sensory neurons caused retraction of $TrkB^+$ afferents from skin and alleviated mechanical allodynia in mouse models of neuropathic pain, suggesting that $TrkB^+$ afferents are necessary and sufficient to convey mechanical allodynia after nerve injury (20). Neubarth et al. further demonstrated a dramatic reduction in the number of Meissner corpuscles upon elimination of brain-derived neurotrophic factor (BDNF), the TrkB ligand, from skin keratinocytes. The finding highlights the importance of skin-derived BDNF in early Meissner corpuscle development (16). To investigate whether skin-derived BDNF is also important for maintenance of mature Meissner corpuscles and for protection against DN, we generated a conditional transgenic mouse that lacked BDNF expression in skin keratinocytes. We also created two skin-specific transgenic mouse lines that either lacked or overexpressed sirtuin 1 (SIRT1), a transcriptional activator of *BDNF*.

SIRT1 is an NAD^+-dependent protein deacetylase which acts as a metabolism sensor in a variety of metabolic processes. Decreased activity or expression levels of SIRT1 have been

observed in various tissues of diabetic patients possibly due to decreased systemic NAD^+ biosynthesis (21–24) or increased NAD^+ degradation (25,26). SIRT1 deacetylates a number of proteins e.g. FoxO, p53 and PGC1α, and regulates transcription of their downstream targets (27). It has also been shown to upregulate brain BDNF expression to mediate neuroprotection against neurodegenerative disease (28,29). Through a diverse approach, we hereby investigated how alterations in epidermal SIRT1 and BDNF underlie the mechanism of mechanical allodynia in animal models of DN.

Results

Loss of Meissner corpuscles is more prominent than loss of free nerve endings and correlates better with severity of mechanical allodynia in mouse models of diabetic neuropathy (DN). The two mouse models of DN used in this study were high-fat diet (HFD) only and HFD combined with low-dose streptozotocin (STZ) (30,31). For the HFD only model, mice were given a HFD for 3-4 months; for the HFD combined with STZ model, mice were given a HFD for 2-3 months, followed by 2 low doses of STZ and continued HFD for another month (Supplemental Figure 1, A and B). After 3-4 months of diet modification/STZ induction, both mouse models developed impaired glucose tolerance (Supplemental Figure 1, C-F). The HFD with low-dose STZ model developed both static and dynamic allodynia (Supplemental Figure 1, I and J), whereas the majority of the HFD model only demonstrated static allodynia (Supplemental Figure 1, G and H). While some HFD only mice also developed dynamic allodynia, the result was not statistically significant compared to their baseline (Supplemental Figure 1H).

Upon examination of the sensory apparatus involved in pain sensation in foot skin, both mouse models of DN demonstrated a profound loss of Meissner corpuscles compared to the control mice (Figure 1, A and B). While the intraepidermal nerve fiber densities (IENFD), which measure predominantly the free nerve endings, were also lower in the DN mice than the control mice, the difference was not as obvious (Figure 1, C and D). Overall, DN caused 60-80% of loss of Meissner corpuscles as opposed to 30% loss of free nerve endings in foot skin of the mice. Furthermore, both Pearson correlation (Figure 1E) and linear regression analysis (Figure 1F) indicated that Meissner corpuscle densities are a better marker of mechanical allodynia than IENFD in mouse models of DN.

Expression of BDNF is decreased in foot skin of DN mice. To identify molecular events that led to Meissner corpuscle loss in DN mice, we performed single-cell RNA-sequencing (scRNA-seq) analyses on foot skin of DN (HFD) and control (control diet [CD]) mice. 7 major cell types were identified after unbiased clustering analysis (Figure 2A). Overall, there were no global changes in cell type proportions or gene expression landscape in DN mice (Figure 2B). We then focused on the expression of the skin-derived neurotrophic factors, which are known to regulate the development or survival of specific cutaneous sensory afferents (32). In mouse foot skin, the most abundant neurotrophic factor was neurturin (NRTN), followed by BDNF. The remaining skin-derived neurotrophic factors were expressed in < 1% of the foot skin cells (Supplemental Figure 2A), and therefore may be less important in supporting cutaneous afferents. NRTN is a member of the glial cell line-derived neurotrophic factor (GDNF)-family ligands (GFLs). Mice lacking NRTN demonstrate loss $P2X3^+$ epidermal afferents due to depletion of $GFR\alpha2^+$ neurons in dorsal root ganglia (DRG) (32,33), whereas mice lacking cutaneous BDNF expression

demonstrate loss of Aδ longitudinal lanceolate endings in hairy skin and Meissner corpuscles in glabrous skin (16,34). In mouse foot skin, BDNF was predominantly expressed by suprabasal keratinocytes (Figure 2C). Notably, BDNF is present only in the epidermis of the foot pads where Meissner corpuscles are located, but not in the intra-pad epidermis which does not contain Meissner corpuscles (Figure 2D). In foot skin of DN mice, there were fewer suprabasal keratinocytes expressing BDNF compared to control mice based on the scRNA-seq data (Figure 2D). The finding was further confirmed by the Western blot analysis, as the protein level of BDNF was also decreased in the foot skin of DN mice (Figure 2, E and F). We speculated that the mechanism of BDNF down-regulation in DN is the decreased enzymatic activity or expression of SIRT1 (21–24), a protein deacetylase involved in BDNF transcription through the TORC1 and CREB pathway (28). Further assessment of SIRT1 deacetylase activity by measuring the acetylation level of its substrate FoxO1 revealed a trend of acetyl-FoxO1 accumulation in the foot skin of DN mice (Figure 2, G and H). However, not all DN mice demonstrated decreased SIRT1 activity since FoxO1 acetylation status may be affected by the acetylase CBP/P300 or other deacetylases e.g. SIRT2 and SIRT3 (35,36). SIRT1 expression levels in foot skin, however, were about the same in DN and control mice (Figure 2, G and I). Interestingly, the percentage and distribution of SIRT1-expressing cells in foot skin (Figure 2J and Supplemental Figure 2B) was very similar to that of BDNF-expressing cells (Figure 2C and Supplemental Figure 2A): SIRT1 was also predominantly expressed by suprabasal keratinocytes. The similarity in epidermal distribution suggests that the two skin-derived molecules may have a functional relationship in supporting mature Meissner corpuscles and protecting them against DN-induced damages.

Diabetic mechanical allodynia is exacerbated by depletion of the BDNF transcriptional regulator SIRT1 in skin keratinocytes. To elucidate the role of skin-derived SIRT1 in the pathogenesis of DN, we generated a conditional epidermal *SIRT1* KO strain *Keratin 5 (K5)-CreER^{T2};SIRT1$^{flox/flox}$*. Tamoxifen was given to adult mice at least 3 months of age to bypass the potential effect of SIRT1 depletion on development of sensory axons. Tamoxifen treatment induced Cre-mediated recombination in basal keratinocytes, producing a non-functional truncated SIRT1 protein due to in-frame deletion of exon 4 (Supplemental Figure 3A) (37). We noticed leaky Cre-mediated expression in basal keratinocytes at approximately half efficiency of the expression induced by full-dose tamoxifen (Supplemental Figure 3B). *SIRT1$^{flox/flox}$* was therefore included as an additional control (Control 1) besides *K5-CreER^{T2};SIRT1$^{flox/flox}$* without tamoxifen (Control 2). K5-Cre-mediated gene recombination, however, was tissue-specific, as expression of the reporter gene was not detected in DRG or spinal cord (Supplemental Figure 3C).

Epidermal *SIRT1* KO mice appeared to be grossly phenotypically normal, except for patchy back hair loss in < 10% of the mice. They did not develop significant mechanical allodynia until after receiving 3 months of HFD; dynamic allodynia in KO mice was more severe than both control groups, whereas static allodynia was only significantly worse than Control 1 (Figure 3, A and B). Notably, while approximately 2/3 of the epidermal *SIRT1* KO mice demonstrated static allodynia, the remaining 1/3 were hyposensitive to pain after diet modification (Figure 3C). Given that hypoalgesia or sensory loss is a feature of later-stage DN (38), the finding suggests that epidermal *SIRT1* KO may be used to model advanced-stage disease. Progression of allodynia was monitored for 7 months after the initiation of HFD. In epidermal *SIRT1* KO mice, both static

and dynamic allodynia worsened over time and peaked at 5 months of diet modification (Figure 3, D and E). Note that Control 2 mice also developed static and dynamic allodynia but to a lesser degree, possibly due to leaky expression of Cre recombinase (Supplemental Figure 3B).

The mechanical pain appeared to be the only sensory domain in foot skin affected by depletion of epidermal SIRT1. There was no noticeable tactile hyposensitivity, thermal hyperalgesia, cold allodynia or abnormal nociception in epidermal *SIRT1* KO mice (Supplemental Figure 4). Depletion of epidermal SIRT1 also did not exacerbate HFD-induced glucose metabolism defects (Supplemental Figure 5).

The SIRT1 activator nicotinamide riboside (NR) was then given to the mice orally to see if it relieved HFD-induced mechanical allodynia. After 4 months of NR treatment, mechanical allodynia in Control 1 mice was ameliorated, whereas epidermal *SIRT1* KO and Control 2 mice continued to have worsened allodynia (Figure 3F) despite having the same level of impaired glucose tolerance as Control 1 (Supplemental Figure 6, A and B).

Depletion of epidermal SIRT1 results in worsened HFD-induced Meissner corpuscle loss, abnormal Meissner corpuscle morphology and large sensory fiber abnormalities. After 3 months of HFD, Meissner corpuscle densities were markedly reduced in epidermal *SIRT1* KO as well as in the Control 2 mice (Figure 4, A and B). The significant mechanical allodynia (Figure 3A) and Meissner corpuscle loss in Control 2 mice indicates that SIRT1 depletion in about half of the skin keratinocytes (Supplemental Figure 3A) is sufficient to exacerbate DN. Of note, NR treatment was able to rescue the Meissner corpuscle loss (Supplemental Figure 6C) but not the

free nerve ending loss (Supplemental Figure 6D) or mechanical pain phenotype (Figure 3F) in KO mice. The finding suggests that regeneration of Meissner corpuscles may rely on a cell-autonomous mechanism that is independent of epidermal SIRT1. According to a recent study by Gangadharan et al., neuropathic pain after nerve injury may result from aberrant reinnervation of tactile end organs such as Meissner corpuscles with nociceptors alone (39). This mechanism may explain why the mechanical pain was slightly worse in KO and Control 2 mice receiving NR than the vehicle (Figure 3F).

Mice lacking epidermal SIRT1 not only demonstrated Meissner corpuscle loss, but also had abnormal Meissner corpuscle morphology. Some Meissner corpuscles had the top oval structure misshaped into a horizontal bar, and others were retreated from papillary dermis and clustered at the base of the dermal epidermal junction (Figure 4C). In contrast to the remarkable Meissner corpuscle alterations, free nerve endings were not affected by depletion of epidermal SIRT1, as the KO and control mice had similar IENFD (Figure 4, D and E).

In addition to Meissner corpuscle pathology, severe axon degeneration of large myelinated (Aß) sensory fibers was noted in subcutaneous nerve bundles of foot skin from epidermal *SIRT1* KO mice (Figure 5A). Since Meissner corpuscles are innervated by Aß axons, the finding suggests that depletion of epidermal SIRT1 may cause retrograde degeneration in Aß mechanosensory axons. The notion was further supported by decreased sensory nerve conduction velocities (NCV) (Figure 5B), which mostly reflects abnormalities in large sensory fibers. Changes in large myelinated sensory axons were also observed in human DN patients: sural nerve biopsies showed an average of 57% reduction in large myelinated axons in DN patients compared to

control individuals. Taken together, results from animal models and human patients both revealed large sensory fiber abnormalities as a common and significant finding of DN.

Knockout of epidermal BDNF, the only neurotrophic factor down-regulated by skin SIRT1 depletion, causes phenotypes similar to knockout of epidermal SIRT1. scRNA-seq was performed on foot skin of epidermal *SIRT1* KO and control mice to identify gene perturbations that might account for the exacerbated DN phenotypes associated with depletion of epidermal SIRT1 (Supplemental Figure 7A). The clustering analysis did not reveal any major changes in cell subpopulations or gene expression landscape (Supplemental Figure 7B). However, targeted analysis of skin-derived neurotrophic factors showed down-regulation of BDNF in epidermal *SIRT1* KO, whereas all the other major neurotrophic factors were in fact up-regulated (Figure 6A). To further characterize the functional relationship between epidermal BDNF and SIRT1, we generated a conditional epidermal *BDNF* KO: *Keratin 5 (K5)-CreER*^{T2}*;BDNF*$^{flox/flox}$. Similar to epidermal *SIRT1* KO, epidermal *BDNF* KO mice developed both static and dynamic allodynia after diet modification (Figure 6, B and C). In addition, their abnormal Meissner corpuscle morphology (Figure 6D), remarkable Meissner corpuscle loss (Figure 6, E and F), relatively unaffected free nerve endings (Figure 6, G and H) and unimpaired glucose tolerance (Supplemental Figure 8, A and B) all resembled the phenotypes of epidermal *SIRT1* KO mice. The results indicate that BDNF and SIRT1 may operate in the same pathway to maintain the function and survival of Meissner corpuscles.

Overexpression of epidermal SIRT1 reverses the phenotypes associated with DN. Since KO of epidermal *SIRT1* worsened the DN phenotypes, we generated an inducible transgenic mouse

overexpressing epidermal SIRT1 to evaluate whether DN phenotypes could be improved. A Tet-On mouse strain epidermal SIRT1OE was created by crossing *K5-rtTA*, a mouse harboring a Keratin 5 promoter-driven reverse tetracycline transactivator (40), with *TREbi-mSIRT1OE/mito-eYFP*, a mouse expressing both mouse SIRT1 protein (mSIRT1) and mito-eYFP under the regulation of a tetracycline response element (TRE) (41). Transgene expression can be induced and visualized when mice are fed with a doxycycline (DOX) diet (Figure 7A). The mice were started on HFD first, and then divided into one group receiving HFD containing DOX and the other group receiving HFD only as the control. Two months after DOX was added to the diet, there was significant improvement of diabetic mechanical allodynia, as the pain thresholds of mice receiving DOX returned to normal (Figure 7B). A complete recovery of Meissner corpuscle loss was also noted (Figure 7, C and D). The mechanism of Meissner corpuscle recovery was most likely due to induction of BDNF expression in foot skin by SIRT1 overexpression (Figure 7, E-G). Notably, free nerve endings in foot skin were also increased by overexpression of epidermal SIRT1 (Figure 7, H and I), while the impaired glucose tolerance was unchanged (Supplemental Figure 8, C and D). The mechanism of increased innervation by free nerve endings, however, was unclear.

Discussion

DN is a sensory disorder with pathology starting as loss of the skin sensory apparatus and gradually progressing to involve the peripheral nerves. In addition to pain and sensory abnormalities, DN patients often have skin manifestations, such as diabetic foot ulcer and diabetic dermopathy (42,43). Cutaneous manifestations may be secondary to neuropathy or a predisposing factor to neuropathy. In the latter case, skin changes caused by diabetes may induce

or accelerate the damage to the sensory apparatus, leading to the development of peripheral neuropathy. Our study supports this notion by demonstrating that neuropathy is exacerbated by depletion of the skin-derived molecule SIRT1 or BDNF.

Skin-derived BDNF has been shown to play a critical role in the early development of skin sensory apparatus, such as Aδ longitudinal lanceolate endings and Meissner corpuscles (16,34). Whether or not skin-derived BDNF remains essential for the maintenance of these sensory apparatus in adulthood is unknown. Data from our study suggest that skin-derived BDNF and its transcriptional regulator SIRT1 may not be required for the survival of the mature Meissner corpuscles under normal conditions, but their deficiency may precipitate the Meissner corpuscle loss associated with aging (44) or diseases.

Deficient neurotrophic support from skin as a pathogenic mechanism of DN has been proposed by earlier studies (45–47). Among the different types of neurotrophic factors, nerve growth factor (NGF), BDNF and GDNF were found to be down-regulated in skin of DN patients, but not neurotrophin 4/5 (NT4/5) or neurotrophin 3 (NT-3) (48). NT-3 was in fact elevated in DN patients in one study (47). Our study results, while in agreement with the other studies about the decreased level of BDNF, showed increased levels of other major neurotrophic factors in skin. Of note, the mRNA in our study was sampled from mouse foot skin, compared to other studies which measured mRNA from biopsies of human thigh or shin skin. The differences between glabrous and hairy skin can perhaps explain the discrepancies about the levels of neurotrophic factors.

Despite mounting evidence implicating neurotrophic factors in the pathogenesis of DN (48), neurotrophin supplementation has not been successful as treatment for sensory neuropathy. Two phase II clinical trials showed that recombinant human NGF administration was effective at ameliorating the symptoms associated with both diabetic polyneuropathy and HIV-related sensory neuropathy. These early studies, however, revealed that painful side effects were dose limiting for NGF (50–52). Injection site hyperalgesia was reported in > 90% of the subjects. In addition, a larger phase III clinical trial failed to confirm the earlier indication of efficacy (52). Recombinant human BDNF has also been evaluated in a small clinical trial for treatment of DN but did not show significant efficacy (53). Why neurotrophic factors do not work for treatment of DN is a complicated issue. Their clinical application is not only limited by the side effect but also the routes of administration and variable bioactivity (52). Alternative approaches, such as small molecule mimetics, topical application and biomaterial-assisted delivery (54), are being developed and may bring a new outlook to the decade-old treatment strategy with neurotrophic factors. Another potential treatment strategy is to stimulate the endogenous overexpression of the neurotrophic factors in a more natural, physiological manner (52). Given the role of SIRT1 in promoting BDNF transcription, stimulation of SIRT1 activity with the NAD^+ precursor nicotinamide riboside (NR) may be a promising option. NR is orally bioavailable, has an excellent toxicity profile (55), and is safe for use in human clinical trials (56,57). It has shown efficacy in animal models (25,26) and would be an excellent choice for treatment of human DN. However, based on our data, its efficacy may be limited when given to subjects with advanced disease. Even if there is a complete recovery of the skin sensory apparatus, the neuropathic pain could remain or become worse (Figure 3F and Supplemental Figure 6C), possibly due to miswiring of regenerated nerves or abnormal end organ targeting (39).

In summary, our findings demonstrate the importance of the skin microenvironment, particularly the levels of epidermal BDNF and its transcriptional regulator SIRT1, in the maintenance of Meissner corpuscles and regulation of mechanical allodynia in animal models of DN. Our results also highlight these skin-derived molecules as promising therapeutic targets for DN given their potential for development of topical therapeutics.

Methods

Animals and treatment

Animals were maintained and handled following the protocols approved by the University of Maryland Baltimore and Johns Hopkins University Animal Care and Use Committee. The C57BL/6J, *K5-CreER*^{T2} (JAX 029155), *SIRT1*$^{flo/flox}$ (JAX 008041) (37), *BDNF*$^{flox/flox}$ (JAX 033689) (58), *K5-rtTA* (JAX 017579) and Ai14 *ROSA26* $^{LSL\text{-}tdTomato}$ (JAX 007914) (59) mouse strains were acquired from the Jackson Laboratory. Generation of *TREbi-mSIRT1OE/mito-eYFP* was described previously (41). Any strain that did not develop impaired glucose tolerance was backcrossed with C57BL/6J for at least 6 generations. Cre-mediated recombination was induced in mice 3-7 months of age by intraperitoneal injection of 2 mg/day tamoxifen (Sigma-Aldrich) diluted with 300 μl corn oil (Sigma-Aldrich) for 3-5 consecutive days. Tamoxifen was given every 2-3 months to maintain Cre expression.

To create HFD only models, mice 3-7 months of age were fed with a HFD containing 36% fat (60% calories from fat), 20.5% protein (15% calories from protein), and 37.5% carbohydrate

(26% calories from carbohydrate) (Bio-Serv, F3282). For KO mice, diet modification was initiated one week after tamoxifen injection. For OE mice, doxycycline (DOX) (Sigma-Aldrich) was added to the HFD at a dose of 200 mg/kg. With regard to the study with nicotinamide riboside (NR) treatment, the experimental group received 300 mg/kg/day NR (ChromaDex) in saline through oral gavage on Monday-Thursday and 600 mg/kg NR on Friday, and the control group received normal saline on Monday-Friday. To create HFD combined with low-dose STZ models, after 2-3 months of receiving HFD the mice were given 75 mg/kg STZ (Sigma-Aldrich) in 0.1M sodium citrate buffer, pH 5.0, through intraperitoneal injection, followed by a second dose of STZ at 50 mg/kg 3 days later (30,31). HFD continued for another month. Mice with random blood glucose ≥ 250 mg/dl (30,31) or fasting blood glucose ≥ 200 mg/dl were considered diabetic (60,61).

Immunohistochemistry and quantification of intraepidermal nerve fiber density (IENFD)

Mouse hind paws were fixed in Zamboni's fixative for 24-48 hours at 4°C and processed as previously described (62). 50 μm floating tissue sections were stained with the primary antibody rabbit anti-protein-gene-product 9.5 (PGP 9.5) (Dako, Z5116, 1:500) overnight and the secondary biotinylated goat anti-rabbit IgG antibody (Vector Laboratories, BA-1000-1.5) for 1 hour, followed by colorimetric detection using the VECTASTAIN ABC-HRP Kit (Vector Laboratories, PK-4000). Quantification of IENFD was performed following the protocol described by Lauria et al (62).

Immunofluorescence staining

Tissue sections were obtained from mouse hind paw skin fixed and embedded following the IENFD protocol. For processing of spinal cord and DRG, mice were first perfused with 4% paraformaldehyde (PFA) in PBS. The nervous tissue was post-fixed in 4% PFA in PBS overnight and cryoprotected in 30% sucrose in PBS before being embedded in Tissue-Tek O.C.T. compound (Sakura Finetek). 30 μm tissue sections were incubated with blocking solution (5% normal goat serum in PBST [0.1% Triton X-100 in PBS]) at room temperature for 30 minutes and then with the primary antibody at 4 °C overnight. After being washed with PBST, tissue sections were incubated with the fluorophore-conjugated secondary antibody at room temperature for 1 hour, washed, stained with DAPI Solution (ThermoFisher, #62248, 1:5000), and mounted with Fluoromount-G (Southern Biotech). Images were acquired by a Carl Zeiss LSM700 or Leica 3i Spinning Disk confocal microscope. Primary antibodies used include rabbit anti-S100 beta (Proteintech, 15146-1-AP, 1:200), rabbit anti-DsRed (Takara, #632496, 1:500) and chicken anti-beta-tubulin 3 (Aves Labs, TUJ-0020, 1:500).

Quantification of Meissner corpuscle density

Confocal images were acquired from 8 hind paw skin sections containing glabrous pads for each mouse and analyzed by the Fiji imaging software. Meissner corpuscle density was defined by the total number of Meissner corpuscles divided by the total length of the 8 paw skin sections measured at the base of the epidermis.

10x single cell RNA sequencing

Mouse paws were collected as biopsies and digested in with 1000 U/ml collagenase and 300 U/ml hyaluronidase (Sigma-Aldrich) and digested for 1.5 hour at 37 °C and 0.25% trypsin-

EDTA (GIBCO) was added for additional digestion for 10 min. Digested tissues were suspended and washed with PBS containing 4% of fetal bovine serum, then filtered through 40 μm cell strainers to make single-cell suspensions. Samples were washed three times and centrifuged at 300 g at 4 °C for 10 min. Cell Hashing was used to label samples from distinct samples (63). Single cell suspensions were labeled with the TotalSeq Hashtag Antibodies (BioLegend) for 30 min on ice. Single cell suspensions were submitted to the Genome Technology Core facility at New York University Langone Medical Center and subjected to 10x genomics sequencing. Analysis of the data was performed using the Seurat V3 package (64).

Western blot analysis

Front paw skin was pulverized in liquid nitrogen and sonicated in RIPA lysis buffer (Sigma-Aldrich) containing protease inhibitor cocktail (Sigma-Aldrich, P8340). The lysates were centrifuged at 12,000 g at 4 °C for 10 min. 10 or 20 μg supernatants were analyzed by Western blot. The band intensity was normalized to β-actin or β-tubulin. Primary antibodies used include rabbit anti-BDNF H-117 (Santa Cruz Biotechnology, sc-20981, 1:200), rabbit anti-BDNF 19-HCLC (ThermoFisher, #710306, 1:500), rabbit anti-SIRT1 (Millipore, 07-131, 1:1000), rabbit anti-acetyl FOXO1 Lys294 (ThermoFisher, PA5-154560, 1:500), mouse anti-FOXO1 3B6 (ThermoFisher, MA5-17078, 1:500), mouse anti-β-actin (Cell Signaling Technology, #3700, 1:1000), rabbit anti-β-tubulin 9F3 (Cell Signaling Technology, #2128, 1:1000), and rabbit anti-vinculin (Cell Signaling Technology, #4650, 1:1000).

Electron microscopy

Tissue was fixed in 4% formaldehyde and 1% glutaraldehyde in phosphate buffer, and processed as previously described (65).

Quantification of Aβ axons in human sural nerve biopsies

Toluidine blue stained semithin sections of sural nerve were imaged using a light microscope. The number of the large myelinated (Aβ) axons (diameter > 5 μm) were manually counted, and their density was determined as the number of Aβ axons divided by the area of the nerve fascicle.

Behavioral testing

Static mechanical allodynia was assessed using von Frey monofilaments (0.02-4 g). Animals were placed on an elevated mesh grid. The test was initiated with a 2 g filament applied gently on the left mid hind paw until the filament started to bend and maintained for ~2 s. A withdrawal response was considered valid only if the hind paw was completely removed from the platform. It was repeated 9 more times at 5-second intervals. The 50% withdrawal threshold was determined using the up-down method of Dixon (41,66).

Dynamic mechanical allodynia was assessed using the dynamic brush assay (67). The adhesive removal (sticky tape) assay, light touch sensitivity assay, Hargreaves test, hot plate assay, acetone evaporation assay and pinprick test were performed following methods previously described by Duan et al (67).

Sensory nerve conduction studies

Sensory NCV were measured from the tail using platinum electrodes, placed adjacent to the nerve, using a 60-80 mA square wave stimulus for 0.1-0.3 msec to obtain near nerve recordings. Orthodromic sensory tail NCV was obtained by placing the G1 (active) electrode at the base of the tail and stimulating 4 cm distally. Sensory responses were averaged from 10 trials until the nerve action potential response was stable. Tail temperature was maintained at 32-37 °C. The onset latency and peak amplitude were measured (41).

Statistical analysis

Statistical analyses were performed by unpaired two-tailed t test (one-tailed for Western blot), one-way or two-way analysis of variance (ANOVA) with Tukey multiple comparison's test. Pearson's correlation and simple linear regression analysis was performed by Prism software, version 9 (GraphPad). A p value of less than 0.05 was considered significant.

Author contributions

CYH and CPJL designed the study and supervised experiments. CYH performed imaging and nerve conduction studies. JO, PN and SR performed immunofluorescence studies. JO, PN, MS, YK and SR performed IENFD analysis. PN and SR performed Western blot analysis, JR performed scRNA-seq. JO, PN and MS performed behavioral testing. JWR, KC, TK assisted with study design and interpretation of results. All authors discussed the results and provided input on the manuscript. CYH wrote the manuscript.

Acknowledgements

This work was supported by National Institutes of Health grant K08NS102468 (to CYH), F30HD105455 (to JR), R01NS119275 (to TK) and R01DK107007 (to JWR), VA Merit review Award BX004895 (to TK), Passano Foundation (to CYH) and Edward Mallinckrodt Jr. Foundation (to CPJL).

References

1. Hicks CW, Selvin E. Epidemiology of Peripheral Neuropathy and Lower Extremity Disease in Diabetes. Curr Diab Rep. 2019;19(10):86.
2. Themistocleous AC, Ramirez JD, Shillo PR, Lees JG, Selvarajah D, Orengo C, et al. The Pain in Neuropathy Study (PiNS): a cross-sectional observational study determining the somatosensory phenotype of painful and painless diabetic neuropathy. Pain. 2016;157(5).
3. Hovaguimian A, Gibbons CH. Diagnosis and Treatment of Pain in Small-fiber Neuropathy. Curr Pain Headache Rep. 2011;15(3):193–200.
4. Malik RA, Veves A, Tesfaye S, Smith G, Cameron N, Zochodne D, et al. Small fibre neuropathy: role in the diagnosis of diabetic sensorimotor polyneuropathy. Diabetes Metab Res Rev. 2011;27(7):678–84.
5. Bertora P, Valla P, Dezuanni E, Osio M, Mantica D, Bevilacqua M, et al. Prevalence of subclinical neuropathy in diabetic patients: assessment by study of conduction velocity distribution within motor and sensory nerve fibres. J Neurol. 1998;245(2):81–6.
6. Herrmann DN, Griffin JW, Hauer P, Cornblath DR, McArthur JC. Epidermal nerve fiber density and sural nerve morphometry in peripheral neuropathies. Neurology. 1999;53(8):1634.
7. Malik RA, Tesfaye S, Newrick PG, Walker D, Rajbhandari SM, Siddique I, et al. Sural nerve pathology in diabetic patients with minimal but progressive neuropathy. Diabetologia. 2005;48(3):578–85.
8. Ørstavik K, Weidner C, Schmidt R, Schmelz M, Hilliges M, Jørum E, et al. Pathological C□fibres in patients with a chronic painful condition. Brain. 2003;126(3):567–78.
9. Beissner F, Brandau A, Henke C, Felden L, Baumgärtner U, Treede R-D, et al. Quick Discrimination of Adelta and C Fiber Mediated Pain Based on Three Verbal Descriptors. PLoS One. 2010;5(9):e12944.
10. Wasner G, Baron R, Jänig W. Dynamic mechanical allodynia in humans is not mediated by a central presynaptic interaction of Aβ-mechanoreceptive and nociceptive C-afferents. Pain. 1999;79(2-3):113-9.
11. Xu Z-Z, Kim YH, Bang S, Zhang Y, Berta T, Wang F, et al. Inhibition of mechanical allodynia in neuropathic pain by TLR5-mediated A-fiber blockade. Nat Med. 2015;21(11):1326–31.
12. Tashima R, Koga K, Sekine M, Kanehisa K, Kohro Y, Tominaga K, et al. Optogenetic Activation of Non-Nociceptive Aβ Fibers Induces Neuropathic Pain-Like Sensory and Emotional Behaviors after Nerve Injury in Rats. eneuro. 2018;5(1):ENEURO.0450-17.2018.
13. Neumann S, Doubell TP, Leslie T, Woolf CJ. Inflammatory pain hypersensitivity

mediated by phenotypic switch in myelinated primary sensory neurons. Nature. 1996;384(6607):360–4.
14. Abraira VE, Ginty DD. The Sensory Neurons of Touch. Neuron. 2013;79(4):618–39.
15. Paré M, Elde R, Mazurkiewicz JE, Smith AM, Rice FL. The Meissner Corpuscle Revised: A Multiafferented Mechanoreceptor with Nociceptor Immunochemical Properties. J Neurosci. 2001;21(18):7236–7246.
16. Neubarth NL, Emanuel AJ, Liu Y, Springel MW, Handler A, Zhang Q, et al. Meissner corpuscles and their spatially intermingled afferents underlie gentle touch perception. Science. 2020;368(6497):eabb2751.
17. Boyette-Davis JA, Cata JP, Zhang H, Driver LC, Wendelschafer-Crabb G, Kennedy WR, et al. Follow-Up Psychophysical Studies in Bortezomib-Related Chemoneuropathy Patients. J Pain. 2011;12(9):1017–24.
18. Peltier AC, Myers MI, Artibee KJ, Hamilton AD, Yan Q, Guo J, et al. Evaluation of dermal myelinated nerve fibers in diabetes mellitus. J Peripher Nerv Syst. 2013;18(2):162–7.
19. Creigh PD, McDermott MP, Sowden JE, Ferguson M, Herrmann DN. In-vivo reflectance confocal microscopy of Meissner's corpuscles in diabetic distal symmetric polyneuropathy. J Neurol Sci. 2017;378:213–9.
20. Dhandapani R, Arokiaraj CM, Taberner FJ, Pacifico P, Raja S, Nocchi L, et al. Control of mechanical pain hypersensitivity in mice through ligand-targeted photoablation of TrkB-positive sensory neurons. Nat Commun. 2018;9(1):1640.
21. Orimo M, Minamino T, Miyauchi H, Tateno K, Okada S, Moriya J, et al. Protective Role of SIRT1 in Diabetic Vascular Dysfunction. Arterioscler Thromb Vasc Biol. 2009;29(6):889–94.
22. Hasegawa K, Wakino S, Simic P, Sakamaki Y, Minakuchi H, Fujimura K, et al. Renal tubular Sirt1 attenuates diabetic albuminuria by epigenetically suppressing Claudin-1 overexpression in podocytes. Nat Med. 2013;19(11):1496–504.
23. Kitada M, Koya D. SIRT1 in Type 2 Diabetes: Mechanisms and Therapeutic Potential. Diabetes Metab J. 2013;37:315–25.
24. Bartoli-Leonard F, Wilkinson FL, Schiro A, Inglott FS, Alexander MY, Weston R. Suppression of SIRT1 in Diabetic Conditions Induces Osteogenic Differentiation of Human Vascular Smooth Muscle Cells via RUNX2 Signalling. Sci Rep. 2019;9(1):878.
25. Trammell SAJ, Weidemann BJ, Chadda A, Yorek MS, Holmes A, Coppey LJ, et al. Nicotinamide Riboside Opposes Type 2 Diabetes and Neuropathy in Mice. Sci Rep. 2016;6:26933.
26. Chandrasekaran K, Najimi N, Sagi AR, Yarlagadda S, Salimian M, Arvas M, et al. NAD+ Precursors Repair Mitochondrial Function in Diabetes and Prevent Experimental Diabetic Neuropathy. Int J Mol Sci. 2022;23(9):4887.
27. Finkel T, Deng C-X, Mostoslavsky R. Recent progress in the biology and physiology of sirtuins. Nature. 2009;460(7255):587–91.
28. Jeong H, Cohen DE, Cui L, Supinski A, Savas JN, Mazzulli JR, et al. Sirt1 mediates neuroprotection from mutant huntingtin by activation of the TORC1 and CREB transcriptional pathway. Nat Med. 2012;18(1):159–65.
29. Jiang M, Wang J, Fu J, Du L, Jeong H, West T, et al. Neuroprotective role of Sirt1 in mammalian models of Huntington's disease through activation of multiple Sirt1 targets. Nat Med. 2012;18(1):153–8.

30. Yorek MS, Obrosov A, Shevalye H, Holmes A, Harper MM, Kardon RH, et al. Effect of diet-induced obesity or type 1 or type 2 diabetes on corneal nerves and peripheral neuropathy in C57Bl/6J mice. J Peripher Nerv Syst. 2015;20(1):24–31.
31. Yorek MS, Obrosov A, Shevalye H, Coppey LJ, Kardon RH, Yorek MA. Early vs. late intervention of high fat/low dose streptozotocin treated C57Bl/6J mice with enalapril, α-lipoic acid, menhaden oil or their combination: Effect on diabetic neuropathy related endpoints. Neuropharmacology. 2017;116:122–31.
32. Albers K, Davis B. The Skin as a Neurotrophic Organ. Neuroscientist. 2007;13:371–82.
33. Heuckeroth RO, Enomoto H, Grider JR, Golden JP, Hanke JA, Jackman A, et al. Gene Targeting Reveals a Critical Role for Neurturin in the Development and Maintenance of Enteric, Sensory, and Parasympathetic Neurons. Neuron. 1999;22(2):253–63.
34. Rutlin M, Ho C-Y, Abraira VE, Cassidy C, Bai L, Woodbury CJ, et al. The Cellular and Molecular Basis of Direction Selectivity of Adelta-LTMRs. Cell. 2014;159(7):1640–51.
35. Daitoku H, Sakamaki J, Fukamizu A. Regulation of FoxO transcription factors by acetylation and protein–protein interactions. Biochim Biophys Acta - Mol Cell Res. 2011;1813(11):1954–60.
36. Jing E, Gesta S, Kahn CR. SIRT2 Regulates Adipocyte Differentiation through FoxO1 Acetylation/Deacetylation. Cell Metab. 2007;6(2):105–14.
37. Li H, Rajendran GK, Liu N, Ware C, Rubin BP, Gu Y. SirT1 modulates the estrogen–insulin-like growth factor-1 signaling for postnatal development of mammary gland in mice. Breast Cancer Res. 2007;9(1):R1.
38. O'Brien PD, Sakowski SA, Feldman EL. Mouse Models of Diabetic Neuropathy. ILAR J. 2014;54(3):259–72.
39. Gangadharan V, Zheng H, Taberner FJ, Landry J, Nees TA, Pistolic J, et al. Neuropathic pain caused by miswiring and abnormal end organ targeting. Nature. 2022;606(7912):137–45.
40. Vitale-Cross L, Amornphimoltham P, Fisher G, Molinolo AA, Gutkind JS. Conditional Expression of K-ras in an Epithelial Compartment that Includes the Stem Cells Is Sufficient to Promote Squamous Cell Carcinogenesis. Cancer Res. 2004;64(24):8804–7.
41. Chandrasekaran K, Salimian M, Konduru SR, Choi J, Kumar P, Long A, et al. Overexpression of Sirtuin 1 protein in neurons prevents and reverses experimental diabetic neuropathy. Brain. 2019;142(12):3737–52.
42. Kiziltan ME, Benbir G, Akalin MA. Is diabetic dermopathy a sign for severe neuropathy in patients with diabetes mellitus? Nerve conduction studies and symptom analysis. Clin Neurophysiol. 2006;117(8):1862–9.
43. Kwok T, Ting PT, Wong EK, Brassard A. Peripheral Neuropathy for Dermatologists: What If Not Diabetic Neuropathy? J Cutan Med Surg. 2013;17(4_suppl):S1–5.
44. García-Piqueras J, García-Mesa Y, Cárcaba L, Feito J, Torres-Parejo I, Martín-Biedma B, et al. Ageing of the somatosensory system at the periphery: age-related changes in cutaneous mechanoreceptors. J Anat. 2019;234(6):839–52.
45. Anand P, Terenghi G, Warner G, Kopelman P, Williams-Chestnut RE, Sinicropi D V. The role of endogenous nerve growth factor in human diabetic neuropathy. Nat Med. 1996;2(6):703–7.
46. Pittenger G, Vinik A. Nerve Growth Factor and Diabetic Neuropathy. Exp Diabesity Res. 2003;4(4):271–85.
47. Brewster WJ, Fernyhough P, Diemel LT, Mohiuddin L, Tomlinson DR. Diabetic

neuropathy, nerve growth factor and other neurotrophic factors. Trends Neurosci. 2017;17(8):321–5.
48. Anand P. Neurotrophic factors and their receptors in human sensory neuropathies. In: NGF and Related Molecules in Health and Disease. Elsevier; 2004. p. 477–92.
49. Kennedy AJ, Wellmer A, Facer P, Saldanha G, Kopelman P, Lindsay RM, et al. Neurotrophin-3 is increased in skin in human diabetic neuropathy. J Neurol Neurosurg & Psychiatry. 1998;65(3):393–395.
50. Apfel SC, Schwartz S, BT A, al et. Efficacy and safety of recombinant human nerve growth factor in patients with diabetic polyneuropathy: A randomized controlled trial. JAMA. 2000;284(17):2215–21.
51. Schifitto G, Yiannoutsos C, Simpson DM, Adornato BT, Singer EJ, Hollander H, et al. Long-term treatment with recombinant nerve growth factor for HIV-associated sensory neuropathy. Neurology. 2001;57(7):1313–1316.
52. Apfel SC. Nerve growth factor for the treatment of diabetic neuropathy: What went wrong, what went right, and what does the future hold? In: Neurobiology of Diabetic Neuropathy. Academic Press; 2002. p. 393–413.
53. Wellmer A, Misra VP, Sharief MK, Kopelman PG, Anand P. A double-blind placebo-controlled clinical trial of recombinant human brain-derived neurotrophic factor (rhBDNF) in diabetic polyneuropathy. J Peripher Nerv Syst. 2001;6(4):204–10.
54. Alastra G, Aloe L, Baldassarro VA, Calzà L, Cescatti M, Duskey JT, et al. Nerve Growth Factor Biodelivery: A Limiting Step in Moving Toward Extensive Clinical Application? Front Neurosci. 2021;15:1–17.
55. Knip M, Douek IF, Moore WPT, Gillmor HA, McLean AEM, Bingley PJ, et al. Safety of high-dose nicotinamide: a review. Diabetologia. 2000;43(11):1337–45.
56. Chen AC, Martin AJ, Choy B, Fernández-Peñas P, Dalziell RA, McKenzie CA, et al. A Phase 3 Randomized Trial of Nicotinamide for Skin-Cancer Chemoprevention. N Engl J Med. 2015;373(17):1618–26.
57. Gale EAM. European Nicotinamide Diabetes Intervention Trial (ENDIT): a randomised controlled trial of intervention before the onset of type 1 diabetes. Lancet. 2016;363(9413):925–31.
58. Rios M, Fan G, Fekete C, Kelly J, Bates B, Kuehn R, et al. Conditional Deletion Of Brain-Derived Neurotrophic Factor in the Postnatal Brain Leads to Obesity and Hyperactivity. Mol Endocrinol. 2001;15(10):1748–57.
59. Madisen L, Zwingman TA, Sunkin SM, Oh SW, Zariwala HA, Gu H, et al. A robust and high-throughput Cre reporting and characterization system for the whole mouse brain. Nat Neurosci. 2010;13(1):133–40.
60. Cantarelli E, Citro A, Marzorati S, Melzi R, Scavini M, Piemonti L. Murine animal models for preclinical islet transplantation. Islets. 2013;5(2):79–86.
61. Furman BL. Streptozotocin-Induced Diabetic Models in Mice and Rats. Curr Protoc. 2021;1(4):e78.
62. Lauria G, Cornblath DR, Johansson O, McArthur JC, Mellgren SI, Nolano M, et al. EFNS guidelines on the use of skin biopsy in the diagnosis of peripheral neuropathy. Eur J Neurol. 2005;12(10):747–58.
63. Stoeckius M, Zheng S, Houck-Loomis B, Hao S, Yeung BZ, Mauck WM, et al. Cell Hashing with barcoded antibodies enables multiplexing and doublet detection for single cell genomics. Genome Biol. 2018;19(1):224.

64. Stuart T, Butler A, Hoffman P, Hafemeister C, Papalexi E, Mauck III WM, et al. Comprehensive Integration of Single-Cell Data. Cell. 2019;177(7):1888-1902.e21.
65. Ho C-Y, Salimian M, Hegert J, O'Brien J, Choi SG, Ames H, et al. Postmortem Assessment of Olfactory Tissue Degeneration and Microvasculopathy in Patients With COVID-19. JAMA Neurol. 2022;79(6):544–53.
66. Chaplan SR, Bach FW, Pogrel JW, Chung JM, Yaksh TL. Quantitative assessment of tactile allodynia in the rat paw. J Neurosci Methods. 1994;53(1):55–63.
67. Duan B, Cheng L, Bourane S, Britz O, Padilla C, Garcia-Campmany L, et al. Identification of Spinal Circuits Transmitting and Gating Mechanical Pain. Cell. 2014;159(6):1417–32.

FIGURE LEGENDS

Figure 1. **Meissner corpuscle density is a better indicator of mechanical allodynia in mouse models of diabetic neuropathy (DN).** (**A**) immunofluorescence images and (**B**) densities of Meissner corpuscles in foot skin from control diet (CD) mice (n = 6), high-fat diet (HFD) mice (n = 7) and HFD mice treated with low-dose streptozotocin (HFD + STZ) (n = 5). Meissner corpuscles are the $S100^+$ rod-shaped terminations present in the dermal papillae near the dermal-epidermal junction (epidermis indicated by the double arrows). (**C**) PGP9.5 immunohistochemistry images and (**D**) intraepidermal nerve fiber densities (IENFD) in foot skin from CD mice (n = 9), HFD mice (n = 9) and HFD mice HFD + STZ mice (n = 5). One-way analysis of variance (ANOVA): **** $p < 0.0001$, ** $p < 0.01$, * $p < 0.05$, ns = non-significant. (**E**) Correlation matrix of Pearson's correlation coefficients (IENFD: n = 14; Meissner corpuscle density: n = 9). (**F**) Simple linear regression analysis. MC: Meissner corpuscle density (IENFD: n = 14; Meissner corpuscle density: n = 9). All scale bars represent 100 μm. Error bars indicate standard error of means (SEM).

Figure 2. Decreased expression of BDNF is noted in foot skin of DN mice. (**A**) UMAP projection of single-cell RNA-seq (scRNA-seq) data from wild-type C57BL6 mouse foot skin colored by cell type annotation (n = 1408). (**B**) UMAP plot of foot skin cells from control-diet (CD) and DN mice receiving high-fat diet (HFD) (n = 2 for each group). (**C**) Scatter plot demonstrating BDNF expression levels in different cell types of mouse foot skin identified by the analysis. Note that in mouse foot skin, BDNF is predominantly expressed by suprabasal epidermal cells (cluster 0). (**D**) Dot plot indicating the differential BDNF expression in suprabasal keratinocytes (cluster 0) between the CD and HFD mice. The size of the circles represents the percentage of BDNF-expressing cells, and the color of the circles represents the

level of BDNF expression. (**E**) A representative Western blot of mouse foot skin lysates with antibodies against BDNF and a loading control. (**F**) Comparison of normalized mature BDNF protein level in foot skin of CD and HFD mice (n = 6 for each group). (**G**) Measurement of SIRT1 deacetylase activity in mouse foot skin by Western blot probing for the acetylated form of its substrate FoxO1. Also shown are blots for total FoxO1, SIRT1 and a loading control, respectively. (**H**) Comparison of acetyl-FoxO1/FoxO1 ratio in foot skin of CD (n = 4) and HFD mice (n = 5). Note the trend highlighted in circles when the outliers (Lane 3 in CD and HFD, respectively) are excluded. Error bars indicate SEM. (**I**) Scatter plot demonstrating SIRT1 expression levels in different cell types of mouse foot skin identified by the scRNA-seq analysis. Student's t-test: * $p < 0.05$, ns = non-significant.

Figure 3. Conditional knockout (KO) of epidermal *SIRT1* in adult mice exacerbates diabetic mechanical allodynia. (**A**) Assessment of static allodynia in epidermal *SIRT1* KO mice (n = 14) and two control groups: Control 1: $SIRT1^{flox/flox}$ (n = 21) and Control 2: $K5\text{-}CreER^{T2};SIRT1^{flox/flox}$ receiving no tamoxifen but showing leaky Cre expression (n = 14). Static allodynia is assessed by the von Frey assay. Note that only mice with normal (1 or 1.4 g) or decreased pain thresholds (< 1 g) are charted. (**B**) Assessment of dynamic allodynia in epidermal *SIRT1* KO (n = 12), Control 1 (n = 11) and Control 2 mice (n = 8). Dynamic allodynia is assessed by the dynamic brush assay. (**C**) Mice with increased pain thresholds (≥ 2g) are charted with the rest of the mice. Epidermal *SIRT1* KO: n = 21; Control 1: n = 22; Control 2: n = 14. (**D**) Time course of static allodynia. (**E**) Time course of dynamic allodynia. (**F**) Time course of static allodynia in mice receiving vehicle or nicotinamide riboside (NR). Epidermal *SIRT1* KO receiving vehicle: n = 9; epidermal *SIRT1* KO receiving NR: n = 6; Control 1 receiving vehicle:

n = 10; Control 1 receiving NR: n = 9; Control 2 receiving vehicle: n = 6; Control 2 receiving NR: n = 6. Error bars indicate SEM. Two-way ANOVA: **** $p < 0.0001$, *** $p < 0.001$, ** $p < 0.01$, ns = non-significant, ## Control 1 receiving 4 months of vehicle vs. NR, $p < 0.01$.

Figure 4. Epidermal *SIRT1* KO shows reduced numbers and abnormal morphology of Meissner corpuscles in foot skin. (**A**) Immunofluorescence images and (**B**) densities of Meissner corpuscles in foot skin from epidermal *SIRT1* KO (n = 7), Control 1 (n = 8) and Control 2 mice (n = 4). Epidermis is indicated by double arrows. Scale bars represent 50 μm. (**C**) Immunofluorescence images showing Meissner corpuscles appearing as a long horizontal bar in epidermis (downward filled arrowheads) or clustered below epidermis (upward arrowhead). Scale bars represent 50 μm. (**D**) PGP9.5 immunohistochemistry images and (**E**) densities of free nerve endings (IENFD) in foot skin from epidermal *SIRT1* KO (n = 6), Control 1 and (n = 8) Control 2 mice (n = 4). Scale bars represent 100 μm. Error bars indicate SEM. One-way ANOVA: ** $p < 0.01$, ns = non-significant.

Figure 5. Large sensory (Aβ) fiber abnormalities and injuries are observed in epidermal *SIRT1* KO mice as well as human DN patients. (**A**) Electron micrographs of subcutaneous nerve bundles in foot skin from epidermal *SIRT1* KO and control mice. n = 3 for Control 1; n = 5 for epidermal *SIRT1* KO. (**B**) Tail sensory nerve conduction studies of epidermal *SIRT1* KO (n = 17), Control 1 (n = 21) and Control 2 (n = 10) mice. Two-way ANOVA: ** $p < 0.01$, ns = non-significant. (**C**) Sural nerve biopsies from human DN (n = 5) and control patients (n = 5). (**D**) Quantification of large myelinated (Aß) axons in sural nerve. Student's t-test: * $p < 0.05$. Error bars indicate SEM.

Figure 6. BDNF is the only neurotrophic factor down-regulated in foot skin of epidermal *SIRT1* KO. KO of BDNF in skin produces the same phenotypes as epidermal *SIRT1* KO. (**A**) Dot plot based on scRNA-seq data (Supplemental Figure 7) indicating the differential expression of neurotrophic factors in keratinocytes of foot skin between Control 1 ($SIRT1^{flox/flox}$) and epidermal *SIRT1* KO mice. The size of the circles represents the percentage of cells expressing a given neurotrophic factor, and the color of the circles represents the expression level of that neurotrophic factor. Similar to epidermal *SIRT1* KO, epidermal *BDNF* KO develop more severe (**B**) static and (**C**) dynamic allodynia than the control after 3 months of HFD. Two-way ANOVA: ** $p < 0.01$, * $p < 0.05$, ns = non-significant. (**D**) Occasional Meissner corpuscles with abnormal morphology (arrowheads) are also seen in epidermal *BDNF* KO mice. (**E**) Immunofluorescence images and (**F**) densities of Meissner corpuscles in foot skin from epidermal *BDNF* KO and control mice. Epidermis is indicated by double arrows. (**G**) PGP9.5 immunohistochemistry images and (**H**) densities of free nerve endings (IENFD) in foot skin from epidermal *BDNF* KO and control mice. All scale bars represent 100 μm. Error bars indicate SEM. Student's t-test: **** $p < 0.0001$, ns = non-significant.

Figure 7. Inducible overexpression of epidermal SIRT1 (OE) rescues the DN phenotypes. (**A**) After one month of doxycycline (DOX) diet, the skin of SIRT1OE mouse can be seen glowing in blue light due to simultaneous expression of a mito-eYFP transgene. (**B**) HFD-associated static allodynia is relieved after 2 months of DOX-induced epidermal SIRT1 overexpression. Two-way ANOVA: ## Control (n = 7) vs. SIRT1OE after 2 months of DOX (n = 7), $p < 0.01$. (**C**) Immunofluorescence images and (**D**) densities of Meissner corpuscles in foot

skin from epidermal SIRT1OE (n = 6) and control mice (n = 6). Epidermis is indicated by double arrows. (**E**) Western blot analysis of foot skin lysates from SIRT1OE (n = 4) and control mice (n = 4). Comparison of (**F**) normalized SIRT1 and (**G**) normalized mature BDNF protein levels in foot skin of SIRT1OE and control mice. (**H**) PGP9.5 immunohistochemistry images and (**I**) densities of free nerve endings (IENFD) in foot skin from epidermal SIRT1OE (n = 6) and control mice (n = 6). All scale bars represent 100 μm. Student's t-test: ** $p < 0.01$, * $p < 0.05$. Error bars indicate SEM.

FIGURE 1

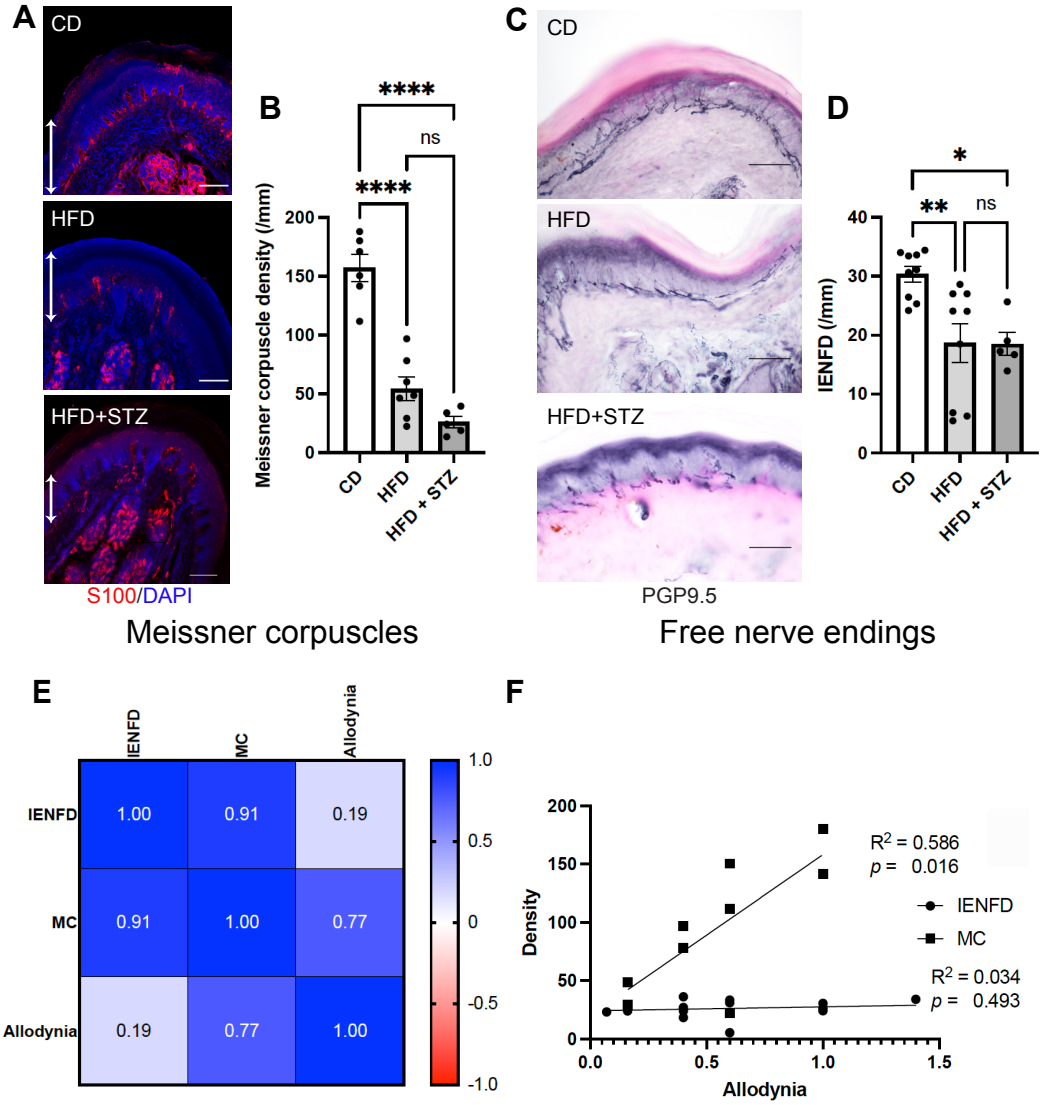
A
CD
HFD
HFD+STZ
S100/DAPI
Meissner corpuscles
B
****
ns
****
Meissner corpuscle density (/mm)
200
150
100
50
0
CD
HFD
HFD + STZ
C
CD
HFD
HFD+STZ
PGP9.5
Free nerve endings
D
*
**
ns
IENFD (/mm)
40
30
20
10
0
CD
HFD
HFD + STZ
E
IENFD
MC
Allodynia
1.00
0.91
0.19
0.91
1.00
0.77
0.19
0.77
1.00
1.0
0.5
0
-0.5
-1.0
F
Density
200
150
100
50
0
0.0
0.5
1.0
1.5
Allodynia
R2 = 0.586
p = 0.016
IENFD
MC
R2 = 0.034
p = 0.493

FIGURE 2

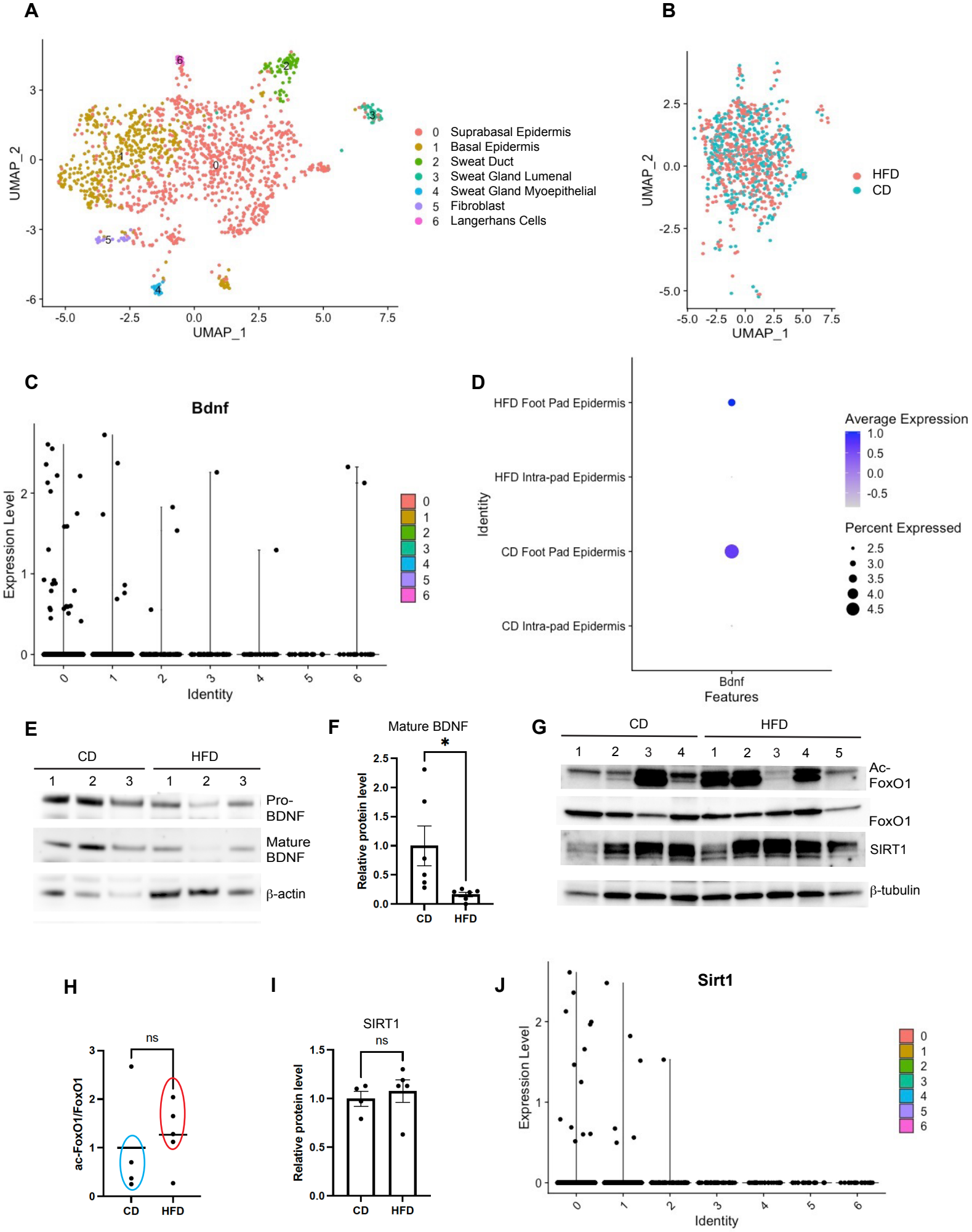
A
UMAP_2
UMAP_1
0 Suprabasal Epidermis
1 Basal Epidermis
2 Sweat Duct
3 Sweat Gland Lumenal
4 Sweat Gland Myoepithelial
5 Fibroblast
6 Langerhans Cells
B
HFD
CD
C
Bdnf
Expression Level
Identity
D
HFD Foot Pad Epidermis
HFD Intra-pad Epidermis
CD Foot Pad Epidermis
CD Intra-pad Epidermis
Identity
Bdnf
Features
Average Expression
Percent Expressed
E
CD
HFD
Pro-BDNF
Mature BDNF
β-actin
F
Mature BDNF
Relative protein level
CD
HFD
G
CD
HFD
Ac-FoxO1
FoxO1
SIRT1
β-tubulin
H
ac-FoxO1/FoxO1
ns
CD
HFD
I
SIRT1
ns
Relative protein level
CD
HFD
J
Sirt1
Expression Level
Identity

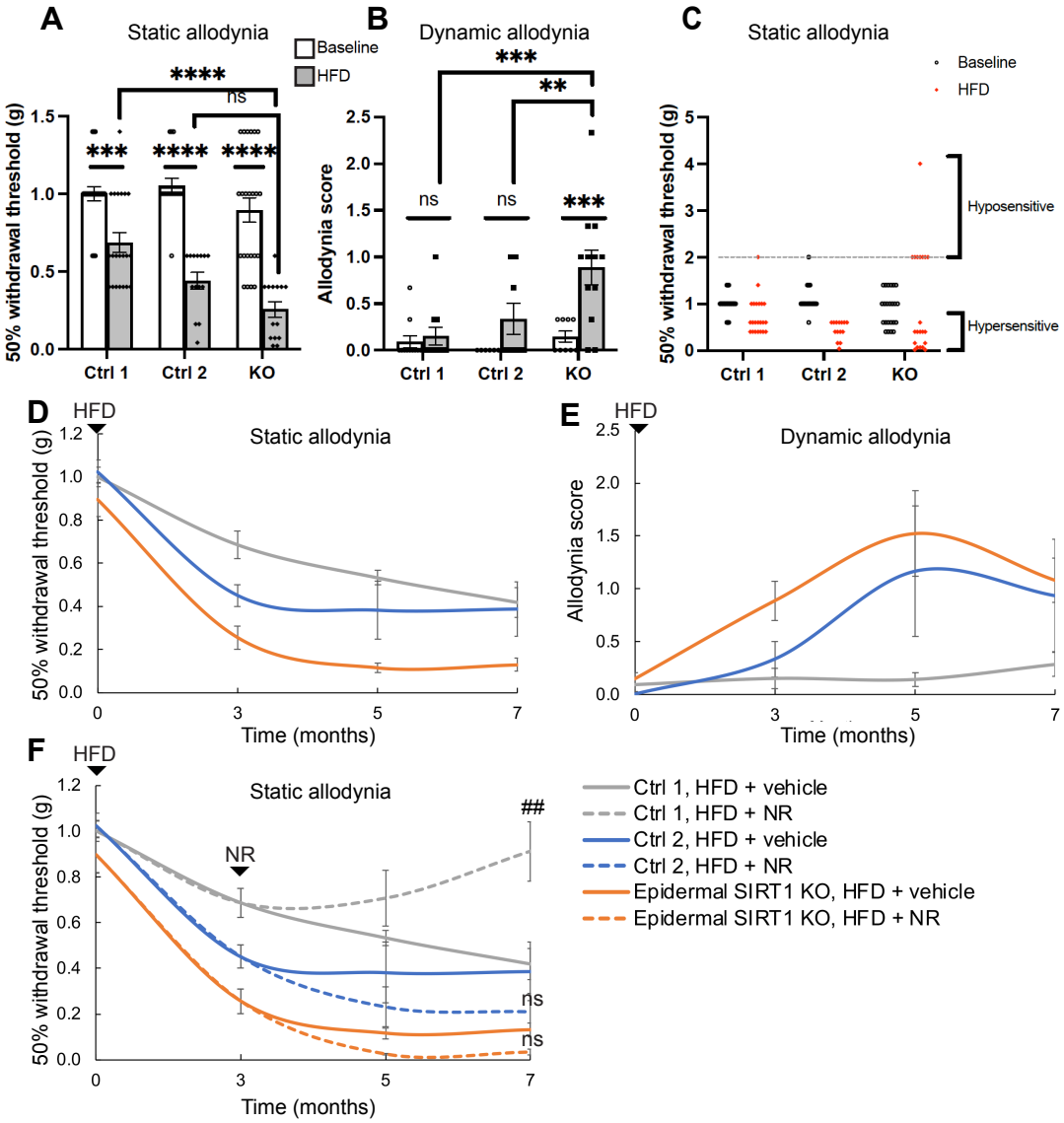
A
Static allodynia
Baseline
HFD
50% withdrawal threshold (g)
Ctrl 1
Ctrl 2
KO
B
Dynamic allodynia
Allodynia score
C
Static allodynia
Hyposensitive
Hypersensitive
D
Static allodynia
Time (months)
E
Dynamic allodynia
F
Static allodynia
NR
##
ns
Ctrl 1, HFD + vehicle
Ctrl 1, HFD + NR
Ctrl 2, HFD + vehicle
Ctrl 2, HFD + NR
Epidermal SIRT1 KO, HFD + vehicle
Epidermal SIRT1 KO, HFD + NR

FIGURE 4

A Meissner corpuscles

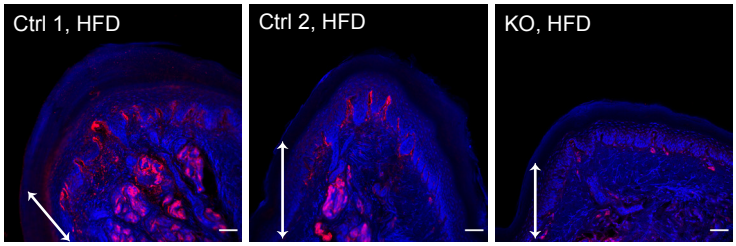

S100/DAPI

B

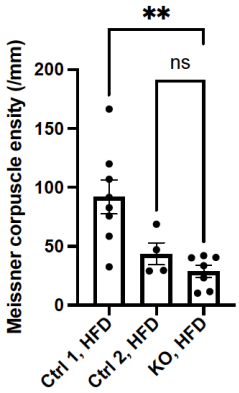

C

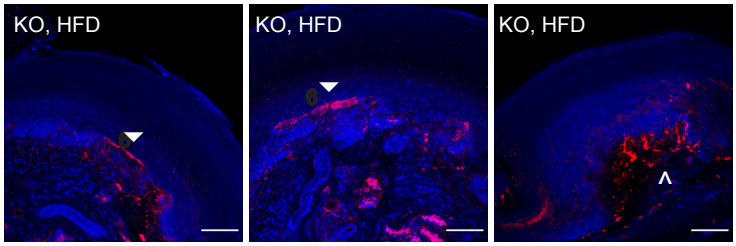

S100/DAPI

D Free nerve endings

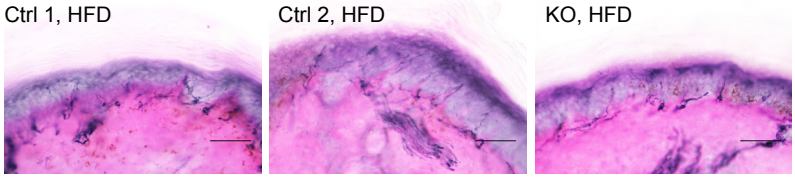

PGP9.5

E

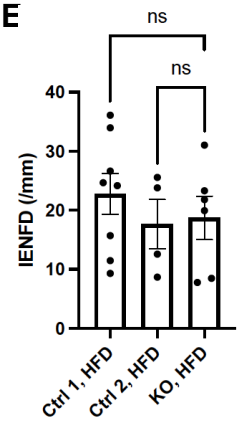

FIGURE 5

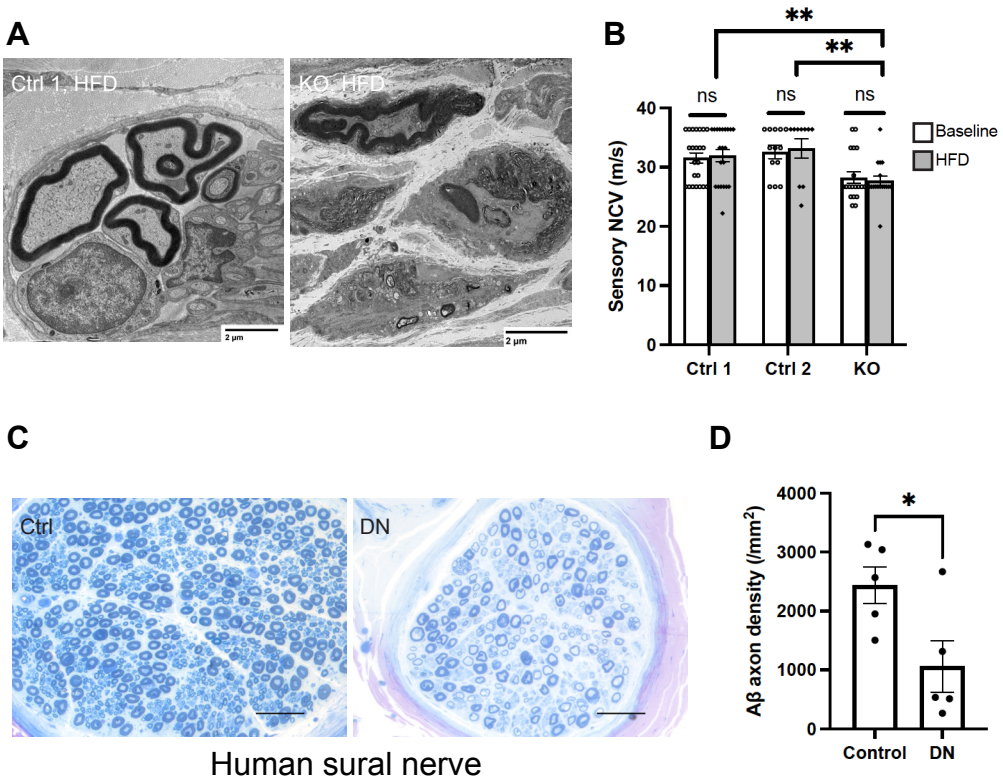
A
Ctrl 1, HFD
KO, HFD
2 µm
2 µm
B
**
**
ns
ns
ns
Sensory NCV (m/s)
40
30
20
10
0
Ctrl 1
Ctrl 2
KO
Baseline
HFD
C
Ctrl
DN
Human sural nerve
D
*
Aβ axon density (/mm²)
4000
3000
2000
1000
0
Control
DN

FIGURE 6

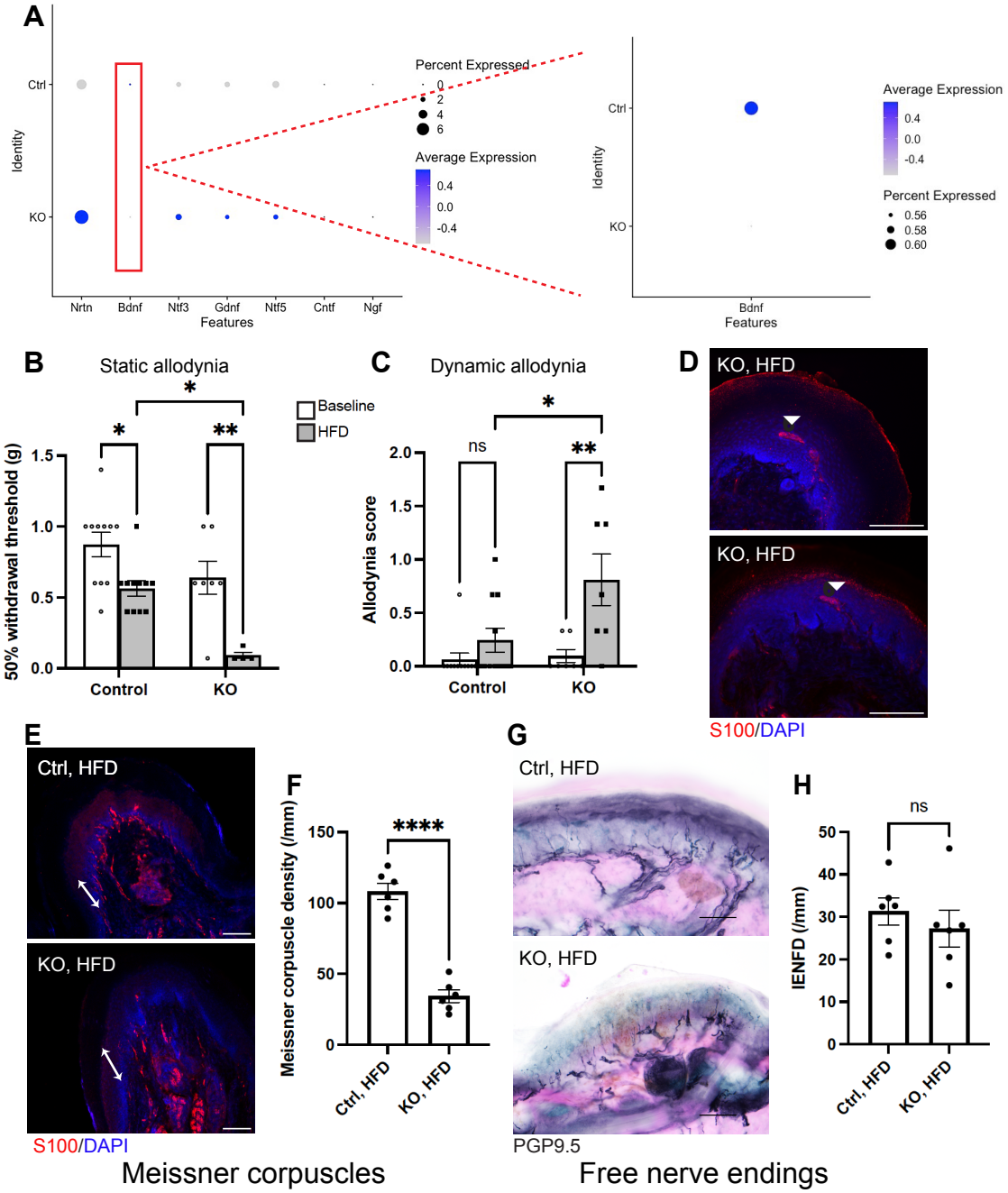

Meissner corpuscles

Free nerve endings

FIGURE 7

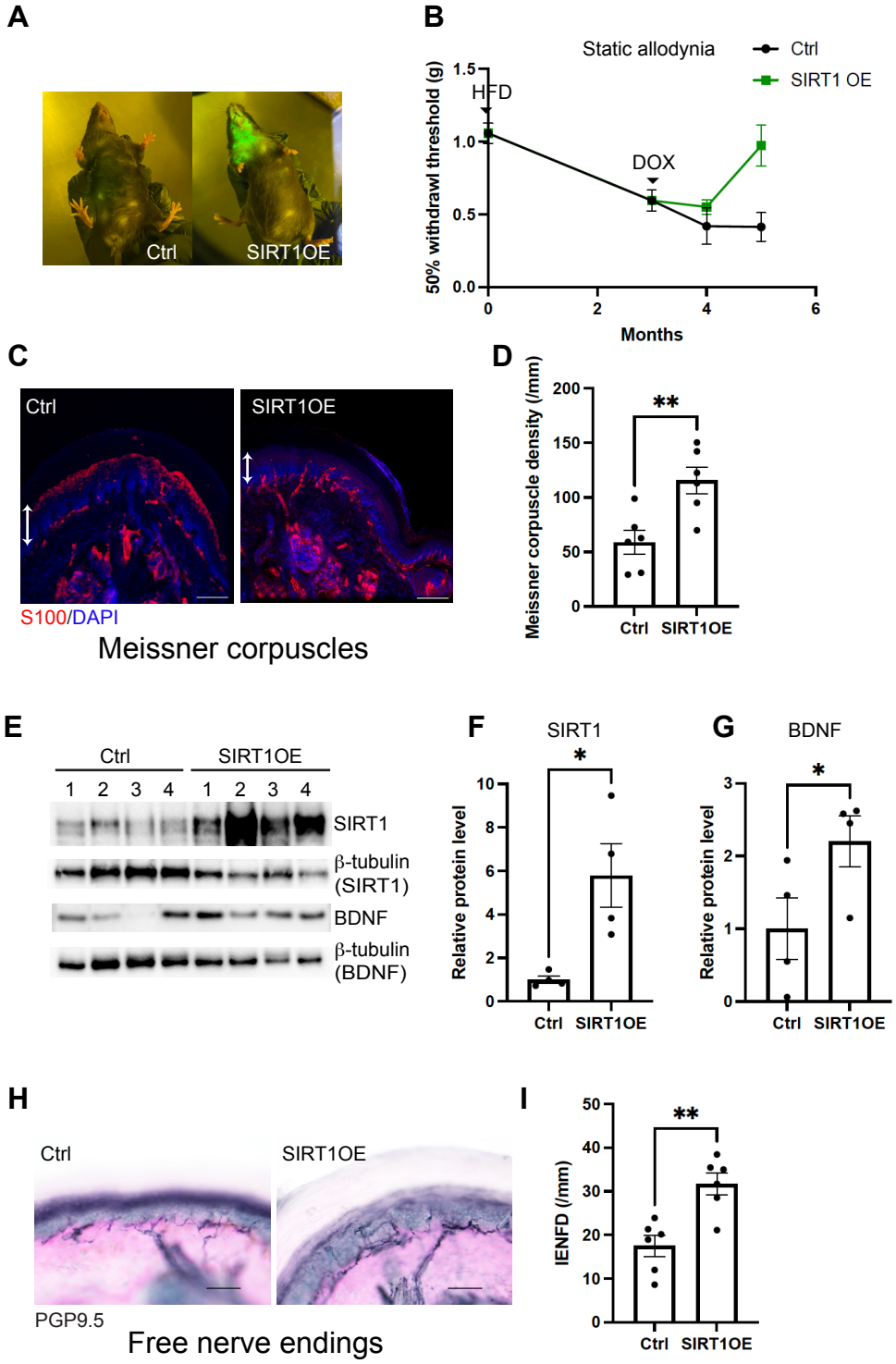
A
Ctrl
SIRT1OE
B
Static allodynia
Ctrl
SIRT1 OE
HFD
DOX
50% withdrawl threshold (g)
1.5
1.0
0.5
0.0
0
2
4
6
Months
C
Ctrl
SIRT1OE
S100/DAPI
Meissner corpuscles
D
Meissner corpuscle density (/mm)
200
150
100
50
0
**
Ctrl
SIRT1OE
E
Ctrl
SIRT1OE
1 2 3 4 1 2 3 4
SIRT1
β-tubulin (SIRT1)
BDNF
β-tubulin (BDNF)
F
SIRT1
*
Relative protein level
10
8
6
4
2
0
Ctrl
SIRT1OE
G
BDNF
*
Relative protein level
3
2
1
0
Ctrl
SIRT1OE
H
Ctrl
SIRT1OE
PGP9.5
Free nerve endings
I
IENFD (/mm)
50
40
30
20
10
0
**
Ctrl
SIRT1OE